


RESEARCH PAPER

Laser ablation–induced synthesis and nonlinear optical characterization of titanium and cobalt nanoparticles

Konda Srinivasa Rao · Rashid A. Ganeev  ·
Ke Zhang · Yue Fu · Ganjaboy S. Boltaev ·
P. S. Krishnendu · Pavel V. Redkin · Chunlei Guo

Received: 8 July 2018 / Accepted: 10 October 2018 / Published online: 22 October 2018
© Springer Nature B.V. 2018

Abstract The studies of third-order nonlinear optical processes (nonlinear saturable absorption, reverse saturable absorption, two-photon absorption, and nonlinear refraction) in the titanium and cobalt nanoparticles synthesized by laser ablation of bulk materials in deionized water, toluene, and ethylene glycol are reported. The nanoparticle suspensions are systematically characterized by absorption spectroscopy, scanning electron microscopy, and Z-scan technique using 800 nm and 400 nm, 60 fs pulses as well as 355 nm, 6 ns pulses. The concurrence of different nonlinear absorption processes in nanoparticle-containing suspensions is discussed. We also demonstrate the optical limiting of these nanoparticles in water using the 800 nm, 60 fs pulses.

Keywords Laser ablation · Titanium nanoparticles · Cobalt nanoparticles · Nonlinear refraction · Nonlinear absorption · Optical limiting · Colloids

K. S. Rao · R. A. Ganeev (✉) · K. Zhang · Y. Fu ·
G. S. Boltaev · P. S. Krishnendu · P. V. Redkin · C. Guo
The Guo China-US Photonics Laboratory, State Key Laboratory
of Applied Optics, Changchun Institute of Optics, Fine Mechanics
and Physics, Chinese Academy of Sciences, Changchun 130033,
China
e-mail: rashid_ganeev@mail.ru

K. Zhang · Y. Fu
University of Chinese Academy of Sciences, Beijing 100039,
China

C. Guo (✉)
The Institute of Optics, University of Rochester, Rochester, NY
14627, USA
e-mail: guo@optics.rochester.edu

Introduction

Formation and characterization of various types of metal nanoparticles (NPs) and quantum dots prepared by chemical and laser ablation methods are the ongoing active areas aimed at their applications in different fields of science (Wang et al. 2015; Diedenhofen et al. 2015; Joos et al. 2017). NPs possess outstanding structural characteristics, attractive functional features, and exceptional nonlinear optical properties compared to those properties of similar bulk materials (Karali et al. 2005; Stepanov 2016). Their distinctive properties were frequently used for optical, electronic, and magnetic applications, as well as for catalysis and biological studies (Ganeev et al. 2004, 2007, 2008).

Currently, laser ablation of the materials immersed in liquid surrounding media has been established as a method for formation of stable NPs (Link et al. 2000; Semaltianos 2010; Ganeev et al. 2005; Hahn et al. 2008), especially those which cannot be synthesized by chemical methods. The majority of studies have been based on the formation of various NPs by focusing the laser pulses on the metal targets immersed in liquids (Shukla et al. 2013). Due to the resonance effect arising from the plasmon resonance of some NPs, their size and shape can be controlled by laser irradiation in various solvents (Mafune et al. 2000; Ali et al. 2015; Tsuji et al. 2005; Jeon and Yeh 1998). Advantages of this method are the high purity of the NPs, variety of materials, and the in situ dispersion of NPs in different liquids tolerating safe and stable control of the colloids. Also, the solvent molecules surrounding NPs can protect them

in some cases from aggregation due to their viscosity and other properties. These studies have also shown the crucial influence of the wavelength and pulse duration of laser radiation on the size and shape of produced NPs (Tsuji et al. 2002; Kabashin and Meunier 2003; Sugiyama et al. 2002; Takami et al. 1999).

Among numerous NPs, the titanium (Ti) and cobalt (Co) species attracted the interest due to their various potential applications (Han et al. 2006). The titanium in its metallic form is not only strong and light-weight but also highly resistant to corrosion. Therefore, it is often used in aerospace and military applications. Ti NPs allow improvement of the radiation resistance. Ti NPs are used in different industrial applications, disease diagnostics, medical imaging, and other fields (Jiang et al. 2018). They have high transparency in the visible range and high UV absorption. Co NPs can be used in medical sensors, coatings, plastics, nanofibers, nanowires, textiles, and high-performance magnetic recording materials. Cobalt oxide NPs can also be used in military applications due to their strong absorption of visible, infrared, and millimeter waves.

Earlier, researchers ablated the bulk Ti rods using nanosecond and femtosecond pulses to produce NPs (Alnassar et al. 2013). The results of studies of various titanium-based NPs formation by laser ablation of Ti rods in liquid environment comprising water, ethanol, 2-propanol, and *n*-hexane were also reported in Reference (Golightly et al. 2006). They have shown the effect of laser fluence on NP characteristics by ablation using a 532-nm Nd: YAG nanosecond laser operating at 10 Hz. In particular, it has been demonstrated that mean particle size and the size distribution increase with growing laser intensity. Ti shows the presence of oxygen in its NPs, which comprised the combination of TiO and TiO₂. Previously, TiO₂ NPs have shown the reverse saturable absorption (RSA) at the wavelength of $\lambda = 780$ nm (Yuwono et al. 2003), and the giant nonlinear optical response at $\lambda = 1064$ nm related with two-photon absorption (2PA) (Gayvoronsky et al. 2005). The mixed two- and three-photon absorption in bulk rutile TiO₂ at $\lambda = 800$ nm was observed using the open-aperture (OA) Z-scan technique (Evans et al. 2012). The formation of Co NPs has been earlier achieved with laser ablation using nanosecond pulses at 355, 532, and 1064 nm (Jin Zhang and Lan 2008; Shukla et al. 2013; Tsuji et al. 2005; Jyothi et al. 2015; Ganeev et al. 2002). Despite those previous works, there have been no reports on the nonlinear absorption and refraction coefficients of Ti

and Co NPs at 800 and 400 nm wavelengths measured using femtosecond pulses. Moreover, we analyze Ti and Co NPs, which were produced during laser ablation of bulk materials using 800 nm, 200 ps pulses for the first time, to the best of our knowledge.

Both Ti and Co are transition metals from the fourth period. Elements in the same period show trends in atomic radius, ionization energy, electron affinity, and electronegativity. Moving left to right across a period, atomic radius usually decreases. This decrease in atomic radius also causes the ionization energy to increase when moving from the left to right across a period. Ti and Co have comparable boiling (3287 and 2927 °C) and melting (1660 and 1495 °C) temperatures, while different densities (4.54 and 8.9 g/cm³). Their main thermal properties are similar. Apart from the abovementioned interest to Ti and Co NPs, the search of peculiarities in the nonlinear optical response can give additional information about their structural properties.

In this paper, we analyze the ablation using picosecond laser pulses and formation of Ti and Co NPs in three liquids. We choose three solvents such as deionized water, toluene, and ethylene glycol (EG) to create the NPs of Ti and Co and control their sizes and shapes. We observe that the size and shape of NPs vary in different surrounding liquids at similar laser ablation conditions. We report the results of measurements of the nonlinear refractive indices, nonlinear absorption coefficients, and saturated intensities of these NPs at the wavelengths of 800 nm and 400 nm (at pulse duration of $t = 60$ fs), as well as 355 nm ($t = 5$ ns). We also discuss our studies of optical limiting (OL) in the suspensions containing these NPs.

Experimental arrangements

The nanoparticles were formed via laser ablation of the Ti and Co sheets immersed in a liquid-containing fused silica cell. The experimental arrangement for laser ablation is shown in Fig. 1a. The incident light was focused on the 1-mm-thick metal sheet using a 100-mm focal length spherical lens, while the 20-mm-thick cell was moved along two directions (*x* and *y*) at a velocity of 0.01 mm s⁻¹. The ablation was performed using uncompressed radiation of Ti: sapphire laser (200 ps, 800 nm; Spitfire Ace, Spectra-Physics) at 1 kHz repetition rate

during 20 to 30 min. The bulk targets were ablated at pulse energy 550 μJ in deionized water, toluene, and ethylene glycol (EG). Before choosing this pulse energy, we ablated the targets with lower pulse energy range. At these conditions, there is a less probability of formation of bubbles in the solvents. However, after increasing the pulse energy up to 550 μJ , significant raise of bubble formation was observed, which directly indicates the worthy production of NPs using 200 ps, 800 nm pulses. The liquid bubbles were produced during ablation of Ti and Co sheets that indicated the vaporization of solvents. The superheated bubbles serve as reaction vessels during NP formation. Atomic and molecular ions most likely come from both the solvent and the Ti/Co during ablation, whereby ion-ion, ion-radical, and ion-molecule interactions take place to form new species. The solvent plays an important role in the variety of NPs produced that is shown by the personalized production of NPs containing carbon and/or oxygen in different solvents.

Once the solution of NPs became prepared, the UV-visible absorption spectroscopy and scanning electron microscopy (SEM) were performed to characterize the suspensions. The UV and visible absorption spectra of NPs were measured using the spectrophotometer (Agilent Technologies). The SEM studies were carried out using the scanning electron microscope (SEM) (S-4800, Hitachi).

Figure 1b shows the standard Z-scan scheme, which was used in these studies. The Ti:sapphire laser (Spectra-Physics, Spitfire Ace) provided 60 fs, 800 nm pulses at 1 kHz repetition rate. These pulses were focused by a 400-mm focal length spherical lens. The thickness of fused silica cells filled with NP suspensions was 2 mm. The OA Z-scan scheme with fully opened iris aperture placed in front of wide area photodiode allowed measurement of the nonlinear absorption of NP suspensions during movement through the focal plane. In the case of closed-aperture (CA) Z-scans, the aperture was narrowed to allow transmitting $\sim 10\%$ of input radiation. The measurements of transmitted radiation in this scheme allowed calculating the nonlinear refractive index of NP suspensions.

The normalized transmittances of our samples were analyzed using the standard fitting procedure to determine their nonlinear absorption coefficients (β) and nonlinear refractive indices (γ). Prior to Z-scan measurements, we characterized the probe beam using a CCD camera (Thorlabs) and confirmed that the beam profile

in the focal area was close to the Gaussian, which is a prerequisite for the analysis of the Z-scan traces using the relations developed for this technique. The corresponding full widths of focused beam at half maximum and $1/e^2$ maximum of intensity distribution were measured to be 42 and 76 μm , respectively. For Z-scan studies, we also used the 400 nm radiation from the same laser by converting 800 nm, 60 fs pulses to the second harmonic in the barium borate (BBO) crystal, as well as 355 nm, 5 ns pulses from Nd:YAG laser (Q-Smart, Coherent).

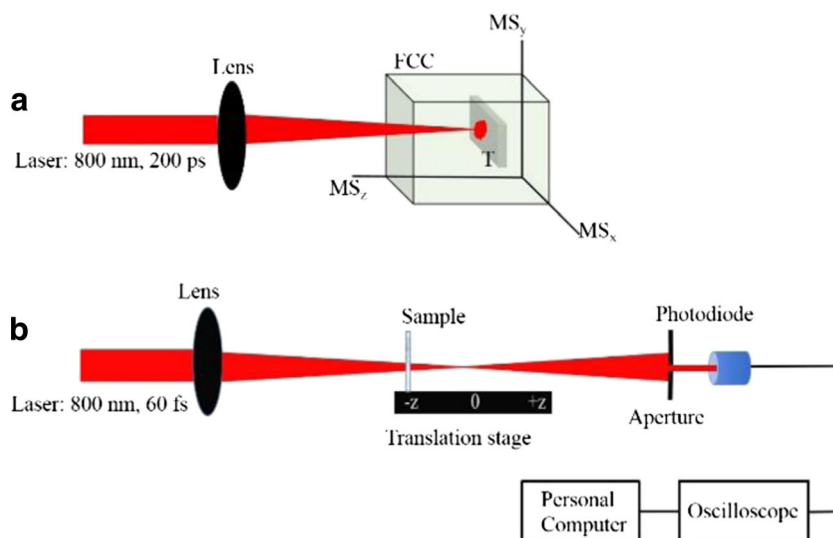
For OL studies, we kept the samples at the focal area of laser beams and measured the transmitted energy as a function of input energy.

Results and discussion

Ablation and characterization of samples

The ablation of bulk materials and formation of NPs in the surrounding media like liquids are the complex processes requiring the analysis of the size-dependent spectral properties of synthesized NPs. Ablation of materials by laser pulses can be considered as a several stage process with different relaxation times. Initially, laser energy is absorbed by electrons in the bulk target. This process is almost instantaneous as the only element governing it is the long-range Coulomb force of the laser field and the charged particles. Then, the heated electrons give their energy to ions, which is a longer process involving the electron-phonon coupling of the material. This process is also relatively fast as compared to atom-atom collisions which redistribute the energy across the volume of the bulk target, melt it, and lead to actual material removal if the energy acquired by the particle is sufficient to leave the surface of the target. Certainly, it can happen that more atoms tend to split off together resulting in the direct removal of NPs from the surface. The next stage is the interaction of the ablated material with the laser pulses and the surrounding medium. In general, interaction with the laser radiation follows the same stages and leads to further fragmentation of NPs. However, the particles have quite different sizes, so their spectral properties are altered greatly, and the destruction of smaller NPs can go slower. The effect of interaction with the surrounding dense medium is twofold. From one hand, the speed of the particles is greatly reduced compared with ablation in air and vacuum,

Fig. 1 **a** Schematic layout for ablation of titanium and cobalt in different liquids. Laser, (800 nm, 200 ps, 1 kHz); lens, $f=100$ mm. FCC, fused silica cell; T, target metal; MS_{xyz} , moving stage. **b** Z-scan scheme



resulting in longer times of exposition to laser radiation. As a result of friction in the medium, the temperature on the surface of ablated NPs increases. On the other hand, the NPs quickly transfer heat to the surrounding medium via heat conductivity, so the actual temperature dynamics may be complicated. Also, the agglomeration of NPs and deposition of particles on NPs can occur with much greater probability in the surrounding medium than in vacuum or air.

In our case, Ti and Co NPs were synthesized by laser ablation of bulk material in water (H_2O), ethylene glycol (C_2H_2), and toluene (C_7H_8) and ethylene glycol (EG) solutions. In the case of toluene and EG solvents, the Ti and Co NPs might contain carbon. Ablation in water led to varying the amount of oxygen incorporation and titanium oxide formation. Very stable and large size NPs were produced due to the high pressures and temperatures of the reaction conditions. After initial analysis, the solutions of NPs were stored in vials. The NPs were analyzed over a period of 1 month and showed stability with some minor fluctuations in sampling. There was no deviation in the composition. The NPs did not undergo further modification within this time. Some of the largest NPs precipitated, and a faint deposit was visible on the bottom of the vials. UV absorption spectra and SEM analysis of the solution revealed that NPs became suspended in solutions without deposition and aggregation. Similar procedure of NPs formation was maintained during bulk Co ablation.

Figure 2 shows the UV-visible absorption spectra of Ti (Fig. 2a–c) and Co (Fig. 2d–f) NPs ablated in water,

toluene, and ethylene glycol solutions. In the case of water and toluene, the Ti NPs show the surface plasmon resonance (SPR) (Fig. 2a, b) at ~ 280 nm, whereas for EG, it is at 457 nm. Moreover, Ti NPs in water and EG possess extended SPR compared to Ti NPs in toluene. The absorbance of Ti NP suspensions in water starts to increase at $\lambda \leq 500$ nm, while for EG, it was at $\lambda \leq 700$ nm. Previously, Barmina et al. reported that Ti NPs have the absorption peak at 530 nm after being ablated by 355 nm, 150 ps pulses in water (Barmina et al. 2010). It was shown earlier that the Ti NPs change their SPR in the case of different composites of materials (Zhao et al. 2015; Torrell et al. 2012; Zhang et al. 2016; Anthony et al. 2008). In the case of Co NPs, the absorption peaks are located at 400 nm and 700 nm (for water), 287 nm (toluene), and 310 nm (EG). Earlier, several researchers shown that the SPR peaks of Co NPs vary based on preparation methods of NPs and composites (Li et al. 2011; Simon et al. 2016; Yashunin and Korytin 2017; Kaminskiene et al. 2013). In our case, the Ti and Co NPs show the different absorption peaks (Fig. 2) in three different liquids, which directly indicates that the size distribution and morphology of produced NPs are different; to identify this, we have further used the SEM analysis.

Figures 3 and 4 and shows the SEM image and size distributions of the Ti and Co NPs ablated in water toluene and EG, respectively. The size distribution of Ti NPs in water, toluene, and EG lies in between 20 and 250 nm, 10 and 100 nm, and 20 and 60 nm, and is corresponding to mean sizes 125 nm, 30 nm, and 40 nm,

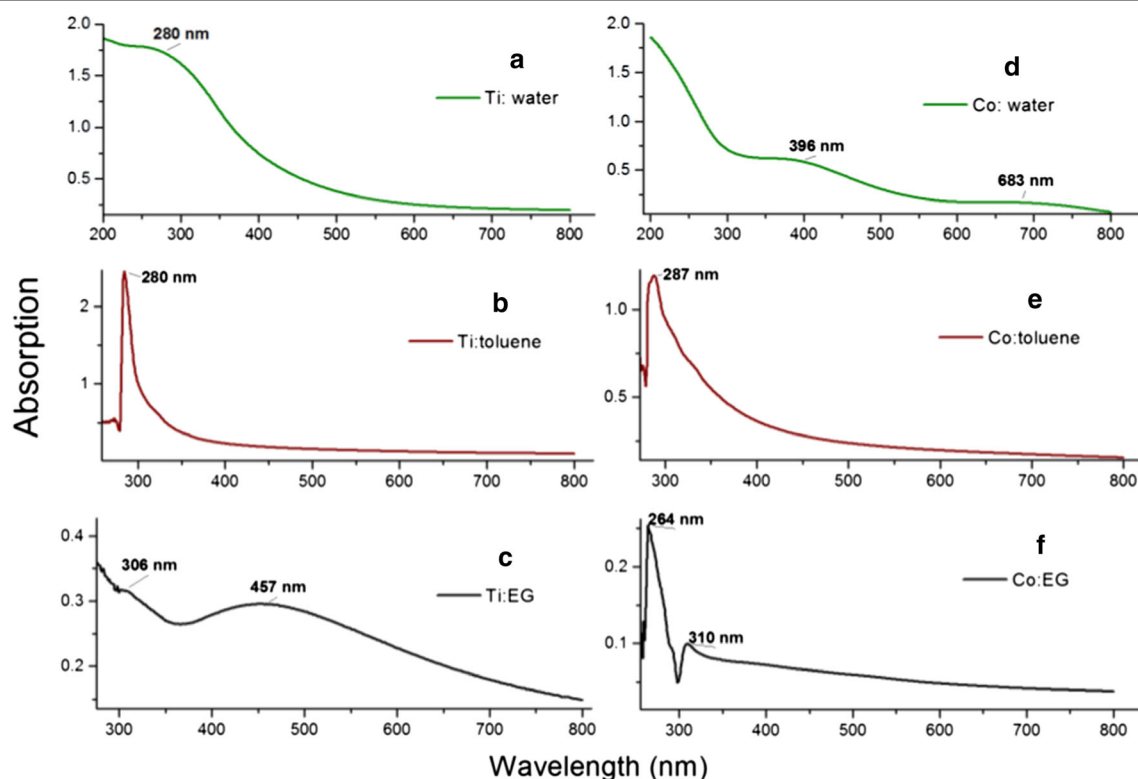


Fig. 2 UV-visible absorption spectra of Ti (a–c) and Co (d–f) NP suspensions ablated in water, toluene, and ethylene glycol solutions

respectively. Whereas, the size distribution of Co NPs synthesized in water was centered at 90 nm. It is important to analyze the processes that determine the morphology of synthesized NPs to control the mean diameter and size distribution of the resulting particles by changing the solvent and pulse energy. Particularly, the sizes of Ti and Co NPs synthesized in water were larger than those prepared in toluene and EG. The surface shape of spherical Ti and Co NPs in water was smooth. Water is a highly polar liquid, and the presence of oxygen leads to formation of the oxides of Ti and Co NPs during laser ablation.

Laser ablation is very efficient in preparation of the NPs and strongly influencing the SPRs compared to the chemical methods of NP formation. One should take into account the high oxidation of NPs when treating the role of solvent, because oxide shell changes the effects of plasmon resonance formation. Such oxide shells are difficult to be destroyed, so small core-shell NPs appear to be stable enough (Simakin et al. 2007). Additionally, the decrease of geometrical cross-section due to fragmentation results in decrease of equilibrium temperature. On the other hand, the melting temperature

for smaller NPs is lower than that of the bulk targets (Castro et al. 1990; Wautelet et al. 2000, 2003; Vall et al. 2001) and is shape-dependent (Wautelet 1998), so the fragmentation or aggregation of such particles continues during further irradiation of NP-containing suspensions.

Optical limiting in NP suspensions

OL of propagating radiation by metal NPs is attractive due to various applications. Previously, considerable efforts have been focused on investigation of the relationship between the OL and nonlinear optical properties of NPs as well as their sizes and shapes. In the following sections, we will show that in the case of nanosecond and femtosecond probe pulses, the Ti and Co NPs can exhibit intensity-dependent transformation from saturable absorption (SA) to RSA. Thus, such NPs may demonstrate strong OL properties in the case of both relatively long and short laser pulses.

In our studies, OL was analyzed using the 800 nm, 60 fs pulses propagating through the suspensions containing Ti and Co NPs in water. Below, we present the OL data for Co NP suspension, while similar behavior

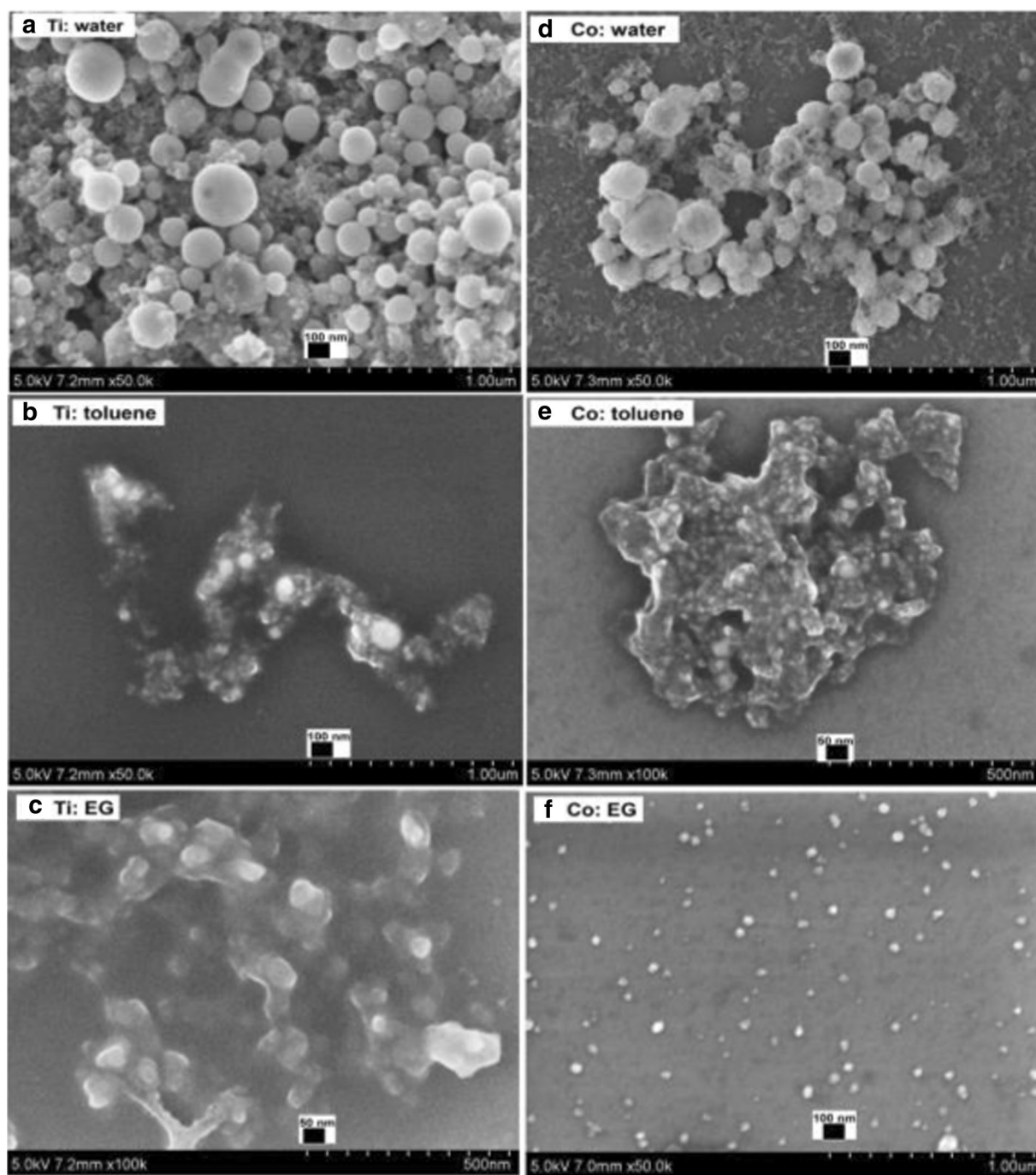


Fig. 3 SEM images of Ti (a–c) and Co (d–f) nanoparticles ablated in deionized water, toluene, and ethylene glycol solutions

was observed for Ti NP suspension as well. The Co NP suspension was placed close to the focal plane of 400-mm focal length lens. We gradually increased the energy of 800-nm pulses and measured the output radiation, which propagated through the 2-mm-thick cell

containing the NP suspension. The linear dependence between input and output pulses was maintained up to the input pulse energy of $\sim 0.08 \mu\text{J}$ (Fig. 5a, filled triangles). The corresponding laser intensity at which OL started to play important role was $3 \times 10^{10} \text{ W cm}^{-2}$.

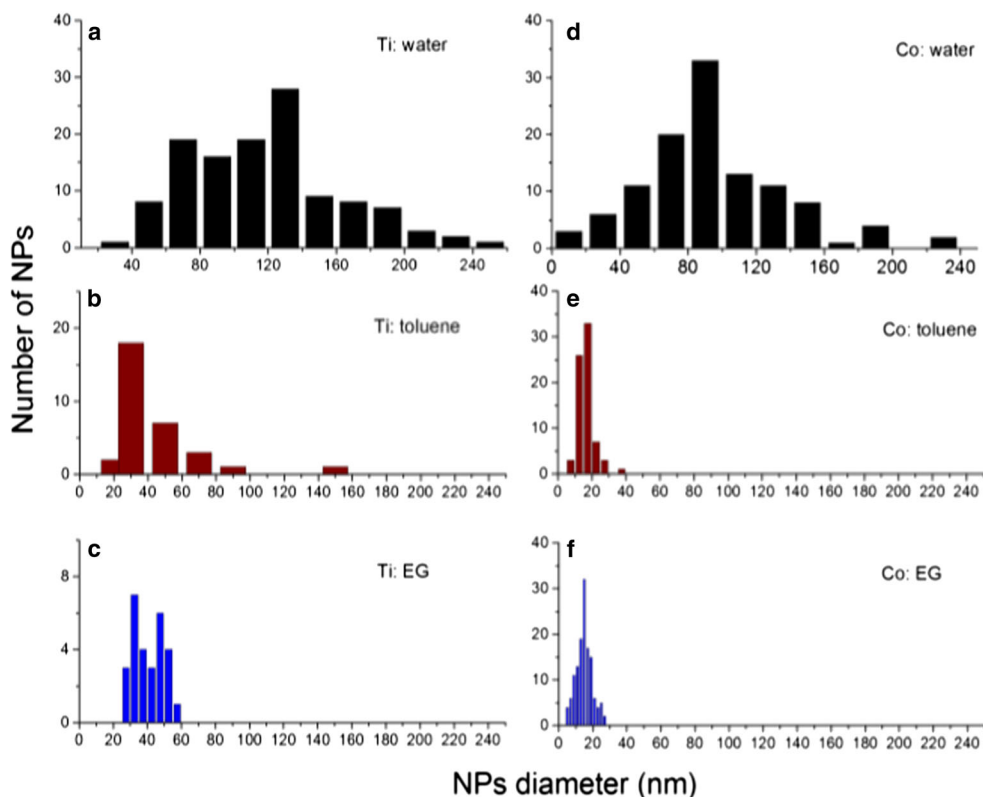


Fig. 4 Histograms of size distribution of the Ti (a–c) and Co (b–d) NPs synthesized during ablation in deionized water, toluene, and ethylene glycol solutions

Further grow of input pulse energy led to the OL of the energy of propagated laser radiation.

The output energy was stabilized at $0.15 \mu\text{J}$. This process was maintained up to the input energy of $1.8 \mu\text{J}$, above which stronger impeding processes worsened the propagation of laser pulses. Similar study in pure water

showed no declination from the linear dependence up to $E_{\text{output}} \sim 0.35 \mu\text{J}$ of output radiation (Fig. 5a, empty circles). At these conditions, the coefficient of OL-induced suppression of propagating radiation was measured to be ~ 2.2 . Further growth of input energy (i.e., above $E_{\text{input}} = 0.4 \mu\text{J}$) in pure water led to white light

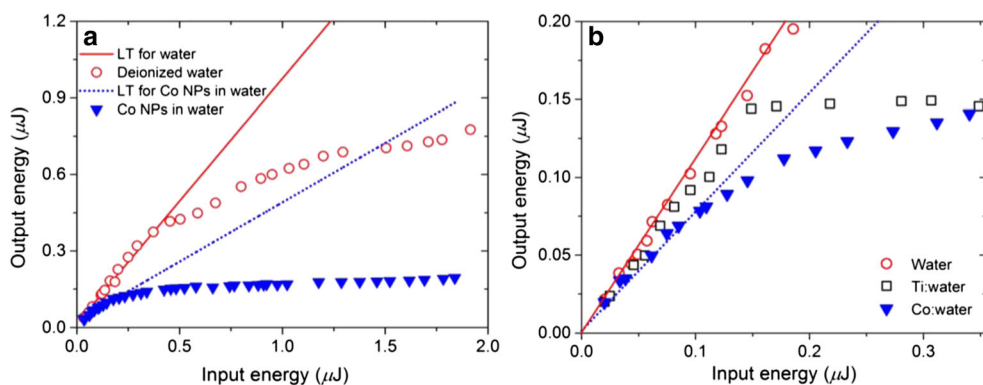


Fig. 5 **a** Optical limiting in Co NPs suspended in water. Filled triangles correspond to Co NPs, and empty circles correspond to pure water. **b** Different behavior of Ti (empty squares) and Co

(filled triangles) NPs at relatively small pulse energies during OL studies. Solid and dotted lines correspond to linear transmittance (LT) for water and Co NPs in water

generation and declination of $E_{\text{input}}/E_{\text{output}}$ ratio from the linear dependence. Nevertheless, at the highest input energy used ($E_{\text{input}} \approx 1.85 \mu\text{J}$), the ~ 3.7 -fold suppression of output pulses was achieved in Co NP suspension compared to pure water.

Meanwhile, considering similar process in Ti NPs suspended in water, we observed an increase of transmittance at the initial stages of this E_{output} (E_{input}) dependence (Fig. 5b, empty squares). This process was attributed to the SA, which with further growth of pulse energy was transformed to the RSA. Then, the latter process became responsible for OL in this NP suspension.

To analyze the nonlinear optical processes responsible for OL, we carried out the systematic studies of these suspensions and determined their γ and β .

Z-scans of samples

The optical nonlinearities of ablated Ti and Co NPs in different liquids were studied using the Z-scan technique at 800 and 400 nm. It is seen from the absorption spectra shown in Fig. 2 that the 800-nm radiation is non-resonant with regard to some possible SPRs of these NPs since there are no absorption peaks in the vicinity of this wavelength. Meanwhile, at 400 nm, all these NPs possess some absorption that can be attributed to some extent to their SPRs.

In the case of OA Z-scan, the normalized transmittance caused by influence of 2PA and RSA is described by Eq. (1) (Sheik-bahae et al. 1989). The case of SA is represented by Eq. (2) (Chapple et al. 1997).

$$T_{2PA} = 1 - \frac{q}{2\sqrt{2}} \quad (1)$$

$$T_{PAZ} = 1 \quad T_{SA}(z) = 1 + \frac{I_o}{I_{sat}(x^2 + 1)} \quad (2)$$

Here, $q = \beta I_0 L_{\text{eff}} / (1 + z^2/z_0^2)$, $x = z/z_0$, $z_0 = k(w_0)^2/2$ is the Rayleigh length, $k = 2\pi/\lambda$ is the wave number, I_0 is the peak intensity in the focal plane, $L_{\text{eff}} = [1 - \exp(-\alpha_0 L)]/\alpha_0$ is the effective length of the medium, w_0 is the beam waist radius at the $1/e^2$ level of intensity distribution, α_0 is the linear absorption coefficient, L is the thickness of our samples, and I_{sat} is the saturated intensity of the medium. In the case of CA Z-scan, the normalized transmittance of nonlinear refraction and absorption (NRA) as well as the combination of

nonlinear refraction (NR) and SA is given by Eqs. (3) and (4) (X. Liu et al. 2001)

$$T_{NRA}(z) = 1 + \frac{2(-\rho x^2 + 2x - 3\rho)}{(x^2 + 1)(x^2 + 9)} \Delta\phi_o \quad (3)$$

$$T_{NR+SA}(z) = 1 + \frac{4x}{(x^2 + 1)(x^2 + 9)} \Delta\phi_o + \frac{I_o}{I_{sat}(x^2 + 1)} \quad (4)$$

Here, $\rho = \beta/2k\gamma$ and $\Delta\phi_o = k\gamma I_0 L_{\text{eff}}$ are the phase change due to nonlinear refraction. The nonlinear optical parameters of our suspensions were calculated by fitting the Eqs. (1)–(4) with the experimental data. The error bars ($\pm 5\%$) of the OA and CA measurements of NP suspensions were the same during the whole set of our experiments. The error bars for determination of the absolute values of nonlinear absorption and refraction coefficients were estimated to be $\pm 25\%$ due to uncertainty in the measurements of the intensity of laser pulses in the focal plane.

Nonlinear optical properties of Ti NPs

Figure 6 shows the Z-scans of Ti NPs measured using 800 nm, 60 fs pulses, as well as the solid curves corresponding to theoretical fits of experimental data. Figure 6a–c and d–f shows the OA and CA Z-scan data corresponding to the Ti NPs in water, toluene, and EG, respectively. Similarly, Fig. 7 presents the Z-scans and theoretical fits in the case of 400 nm, 60 fs probe pulses. The nonlinear optical parameters of Ti NPs at 800 and 400 nm calculated using the Eqs. (1)–(4) are comprised in Table 1. At the 800-nm probe wavelength, the Ti NPs in both water and toluene solutions showed the SA ($\beta = -2.1 \times 10^{-11}$ and $\beta = -2.3 \times 10^{-11} \text{ cm W}^{-1}$, respectively; Figs. 6a, b). In the case of CA, the combined processes of NR and SA were observed in these suspensions that were manifested by larger peaks compared with preceding valleys (Fig. 6d, e). Meanwhile, the influence of SA in Ti NPs in the case of ablation in EG was diminished due to high positive nonlinear absorption of pure solvent (Fig. 6c, f). The negative nonlinear absorption attributed to Ti NPs was smaller compared to the positive nonlinear absorption attributed to EG.

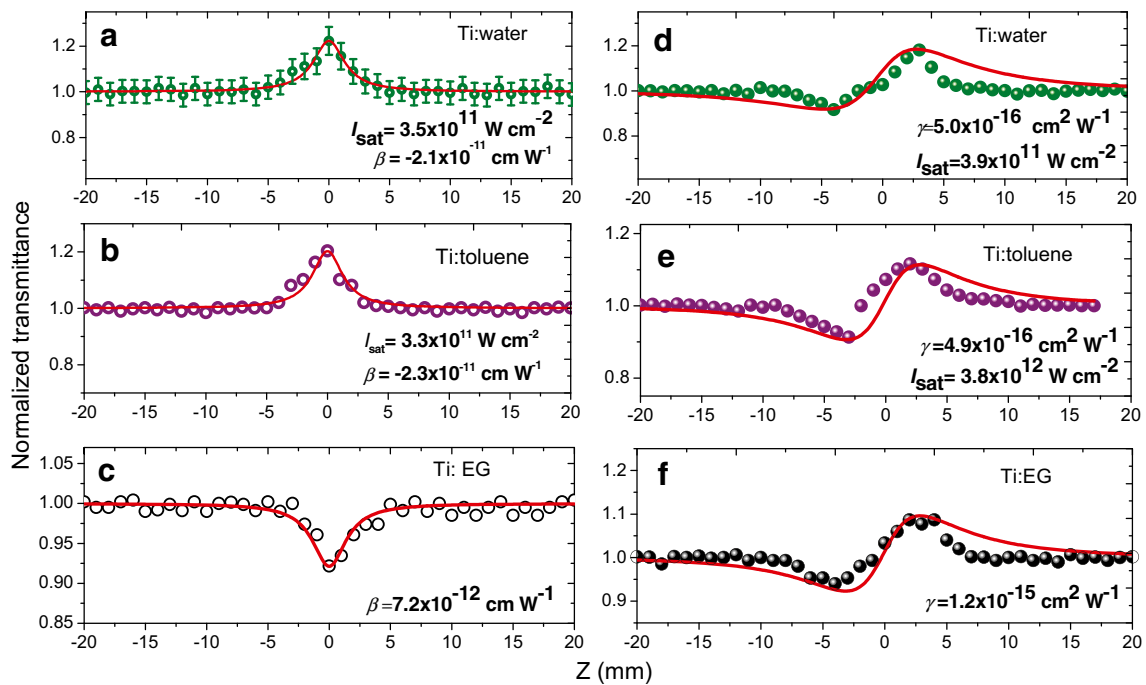


Fig. 6 OA (a–c) and CA (d–f) Z-scans of Ti NPs in different liquids measured using 800-nm radiation. The probe pulse intensities for each of these measurements are presented in Table 1

Overall, the Ti NPs suspended in EG showed the positive nonlinear absorption in the OA scheme. The corresponding nonlinear absorption coefficient in this

suspension was $\beta = 7.2 \times 10^{-12} \text{ cm W}^{-1}$. In the case of CA scheme, the Ti NPs in EG demonstrated pure self-focusing ($\gamma = 1.2 \times 10^{-15} \text{ cm}^2 \text{ W}^{-1}$, Fig. 6f), whereas in

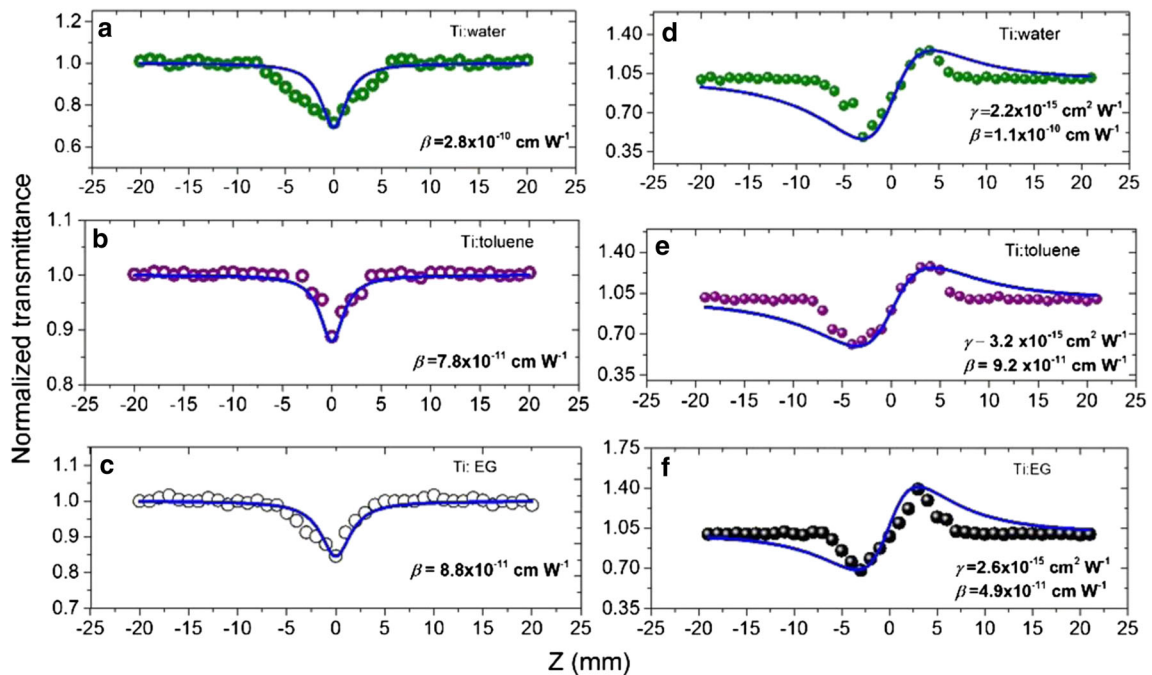


Fig. 7 OA (a–c) and CA (d–f) Z-scans of Ti NP suspensions obtained using 400-nm radiation. $I_0 = 1.5 \times 10^{10} \text{ W cm}^{-2}$

water and toluene solutions, these particles showed the NR + SA processes ($\gamma = 5 \times 10^{-16} \text{ cm}^2 \text{ W}^{-1}$, $I_{\text{sat}} = 3.9 \times 10^{11} \text{ W cm}^{-2}$, and $\gamma = 4.9 \times 10^{-16} \text{ cm}^2 \text{ W}^{-1}$, $I_{\text{sat}} = 3.8 \times 10^{11} \text{ W cm}^{-2}$, respectively). These OA Z-scans demonstrated that the Ti NPs possess SA at 800 nm in the case of 60 fs probe pulses. The values of nonlinear refraction and absorption coefficients of Ti NPs in water were slightly higher compared to Ti NPs in toluene. These studies showed that at relatively small intensities ($7 \times 10^{10} \text{ W cm}^{-2}$), SA is the prevailing process of nonlinear absorption that confirms the behavior of OL curve for Ti NP suspension at small pulse energies (Fig. 6b). Then, with the growth of laser intensity, i.e., at $I_0 > 10^{11} \text{ W cm}^{-2}$, SA process became replaced by RSA leading to OL in this suspension.

In the case of 400-nm probe pulses, the Ti NPs in three solvents showed stronger nonlinear absorption and refraction compared to 800-nm pulses (Fig. 7) due to the closeness of probe pulses to the SPR of Ti NPs. Ti NPs in water demonstrated the largest nonlinear absorption at $\lambda = 400 \text{ nm}$ compared to the other two solvents (compare the data for β , Fig. 7a–c). Both 2PA and RSA could be responsible for positive nonlinear absorption in these conditions. The nonlinear optical characteristics comprised in Table 1 show that the values of nonlinear absorption coefficients for the Ti NPs in these solvents followed the relation $\beta_{\text{water}} > \beta_{\text{EG}} > \beta_{\text{toluene}}$ at $\lambda = 400 \text{ nm}$. In the meantime, the nonlinear refraction indices of Ti NPs suspensions did not follow this rule and were roughly equal to each other (Fig. 7d–f).

Previously, 2PA, SA, and RSA in nanostructured Ni–Ti alloys were investigated at 532 and 1064 nm using nanosecond pulses (Karali et al. 2005). The

dependences of nonlinear absorption on the intensities of laser pulses and sizes of Ni–Ti nanostructures were analyzed. We also measured the normalized variation of transmitted radiation in the case of the Ti NPs suspended in water using 355 nm, 5 ns probe pulses. At small energies ($E = 21 \mu\text{J}$), only the SA occurred in the aqueous suspension containing Ti NPs (Fig. 8, empty triangles). The growth of pulse energy ($E = 54 \mu\text{J}$) led to the change of the sign and magnitude of nonlinear absorption of this suspension in the vicinity of the focal plane (Fig. 7, filled triangles). Further growth of the energy of 355-nm pulses ($E > 0.1 \text{ mJ}$) led to entire disappearance of SA overpassed by RSA.

The nonlinear absorption at $\lambda = 355 \text{ nm}$ in the cases including SA and RSA can be analyzed by the relation $\alpha(I) = \alpha_0 \times I/(I + I_{\text{sat}}) + \beta \times I = \alpha_{\text{SA}} + \alpha_{\text{RSA}}$ for intensity-dependent absorption coefficient (Lee et al. 2009). Here, I is the intensity of laser pulse variable along the z -axis. The nonlinear absorption coefficient consists of two parts: one related with saturable absorption (α_{SA}) and another related with reverse saturable absorption (α_{RSA}). Using this model, one can find the saturation intensity ($I_{\text{sat}} = 2 \times 10^8 \text{ W cm}^{-2}$) for the Ti NP aqueous suspension studied in the case of nanosecond UV pulses (5 ns, 355 nm).

The nonlinear absorption coefficient of this suspension associated with RSA was calculated to be $\beta_{\text{RSA}} = 3.8 \times 10^{-8} \text{ cm W}^{-1}$ (at $\lambda = 355 \text{ nm}$), while the negative nonlinear absorption associated with SA was calculated to be $\beta_{\text{SA}} = -9 \times 10^{-9} \text{ cm W}^{-1}$. The RSA in the medium requires the fulfillment of the following basic criteria: firstly, the material should have an excited-state absorption cross-section larger than the ground-state

Table 1 Nonlinear processes and parameters of Ti NP suspensions calculated using 800 and 400 nm, 60 fs radiation

NPs suspension	Nonlinear process in the case of		$I_0 \text{ (W cm}^{-2}\text{)} \times 10^{10}$	$\gamma \text{ (cm}^2 \text{ W}^{-1}\text{)} \times 10^{-16}$ CA	$\beta \text{ (cm W}^{-1}\text{)} \times 10^{-11}$	$I_{\text{sat}} \text{ (W cm}^{-2}\text{)} \times 10^{11}$	
	OA	CA				OA	CA
Measurements using 800-nm radiation							
Ti: water	SA	NR + SA	7.9	5	−2.1	3.5	3.9
Ti: toluene	SA	NR + SA	6.6	4.9	−2.3	3.3	3.8
Ti: EG	2PA	NRA	10	12	0.72		
Measurements using 400-nm radiation							
Ti: water	RSA	NRA	1.6	22	28		
Ti: toluene	RSA	NRA	1.6	32	7.8		
Ti: EG	RSA	NRA	1.6	26	8.8		

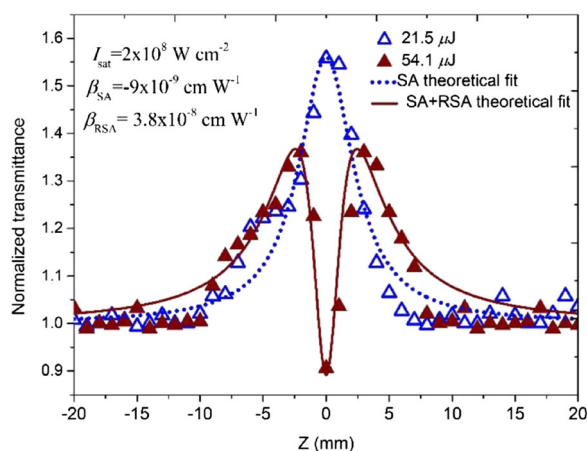


Fig. 8 OA Z-scans of aqueous Ti NP suspension using two energies of 355 nm, 5 ns pulses (21.5 μJ , empty triangles and 54.1 μJ , filled triangles). Fitted curves correspond to the SA (dotted curve) and joint influence of SA and RSA (solid curve)

absorption cross-section, and secondly, the lifetime of the excited state must be long enough. Probably, Ti NPs satisfy the criteria which allow observation of such variations of normalized transmittance using relatively long laser pulses.

SA has been observed previously in various media (glasses doped with semiconductor nanoparticles, dyes, thin polythiophene films, etc.) using long laser pulses in the IR, visible, and UV ranges. We observed this process at two wavelengths and different pulse durations (800 nm, 60 fs and 355 nm, 5 ns) in the case of suspension containing Ti NPs. The appearance of SA in these studies is attributed to bleaching of the ground state at moderate intensities. The dependence of the normalized transmittance in that case may be represented in the form of Eqs. (2) and (1) with negative β . The parameter β of Ti NPs in water in that case is equal to the ratio of the linear absorbance to the saturation intensity ($\beta = -\alpha/I_{\text{sat}}$).

Nonlinear optical properties of Co NPs

Figures 9 and 10 show the OA and CA Z-scans of the Co NPs ablated in water, toluene, and EG in the case of probe 800 and 400 nm, respectively. The corresponding nonlinear optical processes and their parameters are comprised in Table 2. The values of 2PA absorption coefficients of Co NPs are reasonably moderate compared to nonlinear parameters of recently reported materials such as semiconductors, perovskites, and other

2D materials (Liu et al. 2017; Chelnokov et al. 2009; Liu et al. 2018; Films et al. 2015).

In the case of OA Z-scans, the Co NPs in water, toluene, and EG demonstrated the 2PA or RSA (800 nm) and RSA (400 nm), whereas CA scheme revealed the nonlinear refraction and absorption. The values of γ and β for Co NPs in toluene ($I_0 = 2.5 \times 10^{11} \text{ W cm}^{-2}$) were slightly higher than those for Co NPs in water ($I_0 = 2.7 \times 10^{11} \text{ W cm}^{-2}$) and EG ($I_0 = 2.2 \times 10^{11} \text{ W cm}^{-2}$). It was expected to be high values of γ and β for Co NPs in EG due to their small size of distribution. The nonlinear absorption studies of Co NP suspensions showed that this process was observed at both wavelengths (800 nm and 400 nm).

Our studies demonstrated that some nonlinear optical parameters of NP suspensions could be dependent on the probe pulse duration. Earlier, Amekura et al. reported that Co NPs show the broad absorption peak at 4 eV ($\sim 310 \text{ nm}$) (Amekura et al. 2004). Shukla et al. demonstrated synthesis of the Co NPs ablated in toluene, analyzed their optical limiting properties with nanosecond laser pulses (532 nm), and revealed that Co NPs possess strong RSA in OA scheme (Shukla et al. 2013). In the case of CA scheme, they have shown that Co NPs in toluene demonstrated self-defocusing. Previously, RSA and self-defocusing were observed at 532-nm wavelength in Co-doped polymers using picosecond laser pulses (Ganeev et al. 2002) [31]. However, in our case, for both wavelengths (i.e., at 800 nm and 400 nm), the Co NPs ablated in water and toluene showed the 2PA and RSA, respectively, while demonstrating the self-focusing process.

As it is shown in Fig. 2, the absorption peak of Co NPs in water demonstrates the SPR at 400 nm (Fig. 2d). These NPs have stronger linear absorption at 400 nm compared to 800 nm. In our case, at both 800 and 400 nm wavelengths, the Co NPs in three solvents show nonlinear refraction and absorption indicating the self-focusing condition while using short (60 fs) pulses. The nonlinear optical parameters of Co NPs in water have higher values at 800 nm compared to 400 nm. However, the smallest NPs (in the case of toluene (SPR peak at 287 nm, see Fig. 2e) and EG (SPR peak at 310 nm, see Fig. 2f)) have strong nonlinear absorption and refraction coefficients at resonance wavelength (400 nm). The highest values of β ($210 \times 10^{-12} \text{ cm W}^{-1}$) and γ ($21 \times 10^{-16} \text{ cm}^2 \text{ W}^{-1}$) are achieved for Co NPs in EG. These measurements of the nonlinearities of the Co NPs suspended in different liquids (which have smallest size)

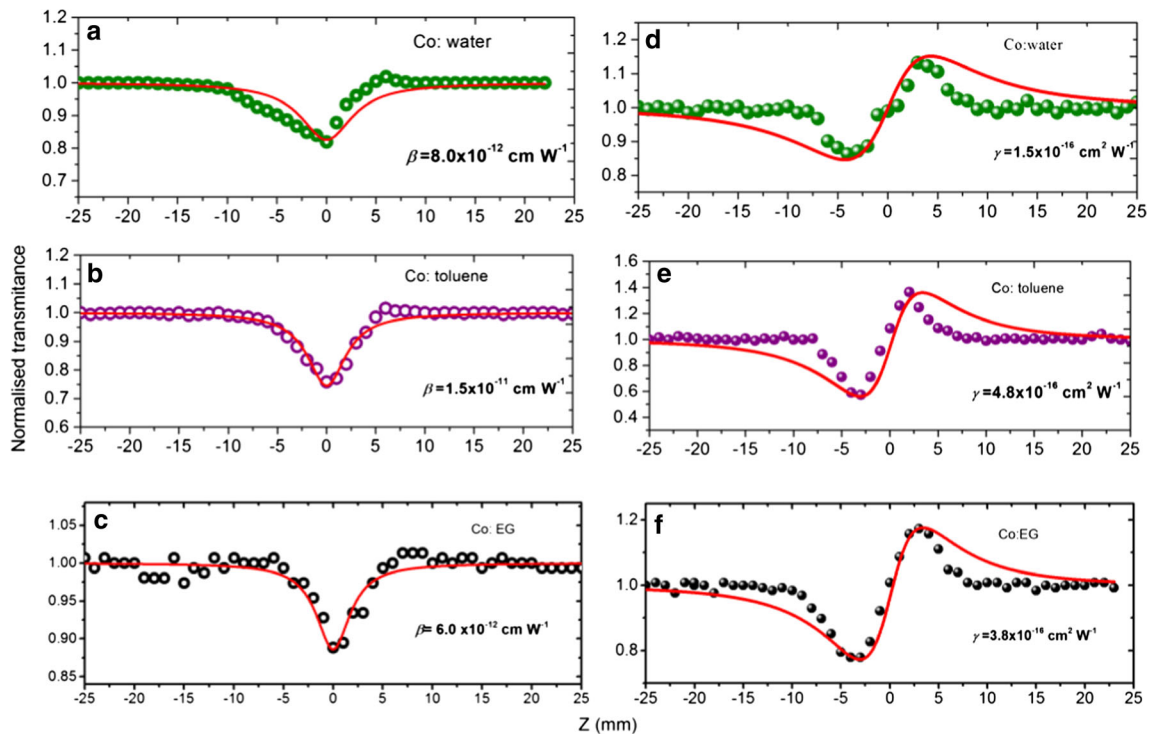


Fig. 9 OA (a–c) and CA (d–f) Z-scans (800 nm, 60 fs) of the Co NPs obtained during ablation in water (a, d), toluene (b, e), and ethylene glycol (c, f), respectively. The corresponding nonlinear optical parameters are shown on the graphs

reveal that they possess strong nonlinear refraction and absorption at resonance wavelengths.

To best of our knowledge, previously, there are no studies on the Ti and Co NPs in the femtosecond range

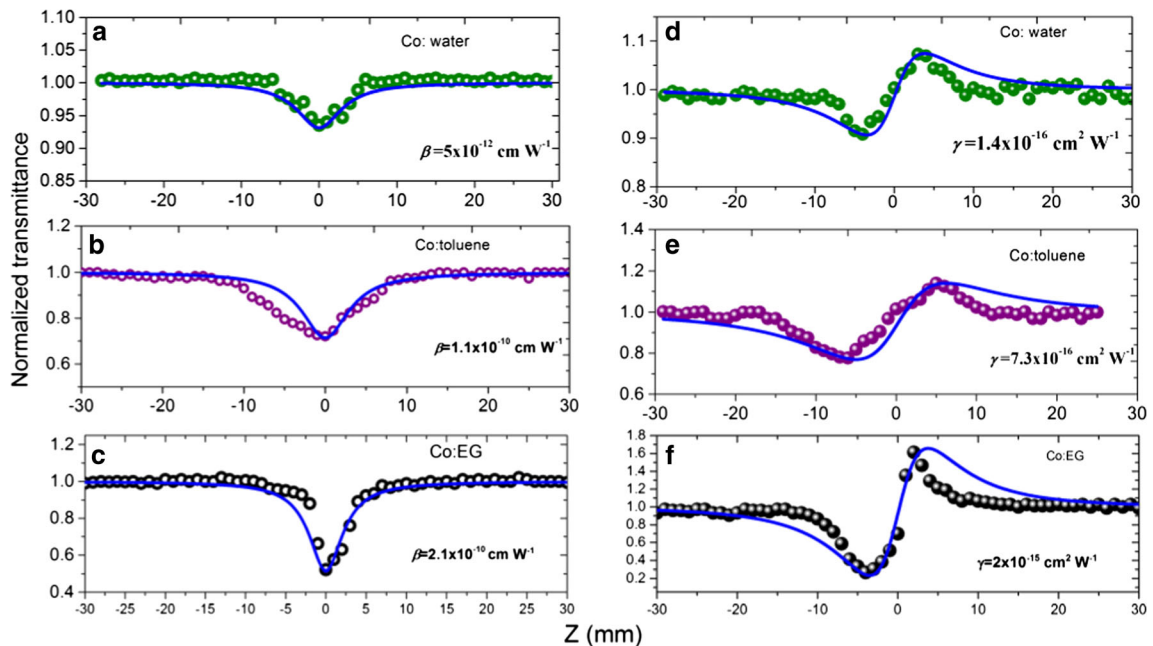


Fig. 10 OA (a–c) and CA (d–f) Z-scans (400 nm, 40 fs) of Co NPs in water (a, d), toluene (b, e), and ethylene glycol (c, f), respectively. The corresponding nonlinear optical parameters are shown on the graphs

Table 2 Obtained nonlinear process from OA and CA Z-scans (800 nm, 400 nm) and their parameters of Co NPs in water, toluene, and ethylene glycol

NP suspension	Nonlinear process in the case of		I_0 (W cm ⁻²) × 10 ¹¹	γ (cm ² W ⁻¹) × 10 ⁻¹⁶	β (cm W ⁻¹) × 10 ⁻¹²
	OA	CA			
Measurements using 800 nm radiation					
Co:water	2PA	NRA	2.7	1.5	8
Co:toluene	2PA	NRA	2.5	4.8	15
Co:EG	2PA	NRA	2.2	3.8	6
Measurements using 400 nm radiation					
Co:water	RSA	NRA	2.2	1.6	5.0
Co:toluene	RSA	NRA	0.3	7.3	110
Co:EG	RSA	NRA	0.5	21	210

that were reported. The aim of the present work was to understand the nonlinear optical properties of Ti and Co nanoparticle in suspensions. Our results have shown the strong high nonlinear optical responses and optical limiting of studied nanoparticles. These nanoparticles can be a good candidate for the generation of higher-order harmonics as compared to the plasmas from ablated bulk metals. Thus, based on the nonlinear optical characteristics, we can predict the possibility of efficient harmonics generation in these nanoparticles.

Conclusions

Titanium and cobalt nanoparticles were synthesized using laser ablation technique in different liquid solvents (water, toluene, and ethylene glycol) using 200 ps pulses. We systematically investigated the structural and nonlinear optical properties of Ti and Co NPs in these suspensions. Studies of optical limiting of suspensions showed that they could be considered as the effective limiters of 800 nm, 60 fs pulses. The origin of this process was analyzed using different experimental conditions. The third-order nonlinear optical properties of NPs were studied using the 60 fs pulses at two wavelengths. Ti and Co NPs showed SA and 2PA at 800 nm and RSA at 400 nm. At 800 nm, in the case of CA Z-scans, the joint influence of nonlinear refraction and SA was observed for Ti NPs in water and toluene, whereas nonlinear refraction and positive absorption were dominated in the ethylene glycol solution containing these NPs. The Ti and Co NPs showed positive nonlinear refraction at both 800 and 400 nm. The Ti

NPs ablated in water demonstrated the SA in the case of 355 nm, 5 ns pulses at lower energies and RSA at larger energies. The measurements of Z-scans and optical limiting demonstrated that the Ti NPs have higher nonlinear absorption and refraction coefficients as compared to Co NPs.

Funding information The financial support from the National Key Research and Development Program of China (2017YFB1104700) and National Natural Science Foundation of China (Grant Nos. 91750205 and 61774155) is appreciated. R.A.G. thanks the financial support from the Chinese Academy of Sciences President's International Fellowship Initiative (Grant No. 2018VSA0001).

Compliance with ethical standards

Conflict of interest The authors declare that they have no conflict of interest.

References

- Ali M, Remalli N, Yehya F, Chaudhary AK, Srikanth VVSS (2015) Picosecond laser induced fragmentation of coarse Cu₂O particles into nanoparticles in liquid media. *Appl Surf Sci* 357:1601–1605. <https://doi.org/10.1016/j.apsusc.2015.10.041>
- Alnassar SI, Akman E, Oztoprak BG, Kacar E, Gundogdu O, Khaleel A, Demir A (2013) Study of the fragmentation phenomena of TiO₂ nanoparticles produced by femtosecond laser ablation in aqueous media. *Opt Laser Technol* 51:17–23. <https://doi.org/10.1016/j.optlastec.2013.02.013>
- Amekura H, Kitazawa H, Umeda N, Takeda Y, Kishimoto N (2004) Nickel nanoparticles in silica glass fabricated by

- 60 keV negative-ion implantation. Nucl Inst Methods Phys Res B 222:114–122. <https://doi.org/10.1016/j.nimb.2004.01.214>
- Anthony JK, Kim HC, Lee HW, Mahapatra SK, Lee HM, Kim CK, Kim K, Lim H, Rotermund F (2008) Particle size-dependent giant nonlinear absorption in nanostructured Ni-Ti alloys. Opt Express 16(15):11193–11202. <https://doi.org/10.1364/OE.16.011193>
- Barmina EB, Stratakis E, Fotakis C, Shafeev GA (2010) Generation of nanostructures on metals by laser ablation in liquids: new results. Quantum Electron 40(11):1012–1020. <https://doi.org/10.1070/QE2010v04n11ABEH014444>
- Castro T, Reifemberger R, Choi E, Andres RP (1990) Size-dependent melting temperature of individual nanometer-sized metallic clusters. Phys Rev B 42(13):8548–8557
- Chapple PB, Staromlynska J, Hermann JA, McKay TJ, McDuff RG (1997) Single-beam Z-scan: measurement techniques and analysis. J Nonlinear Opt Phys Mater 6(3):251–293. <https://doi.org/10.1142/S0218863597000204>
- Chelnokov EV, Bityurin N, Ozerov I, Marine W (2009) Two-photon pumped random laser in nanocrystalline ZnO two-photon pumped random laser in nanocrystalline ZnO. Appl Phys Lett 89(171119):171119. <https://doi.org/10.1063/1.3237089>
- Diedenhofen SL, Kufer D, Lasanta T, Konstantatos G (2015) Integrated colloidal quantum dot photodetectors with color-tunable plasmonic nanofocusing lenses. Light: Sci Appl 4(2014):1–7. <https://doi.org/10.1038/lsa.2015.7>
- Evans CC, Bradley JDB, Martí-Panameño EA, Mazur E (2012) Mixed two- and three-photon absorption in bulk rutile (TiO₂) around 800 nm. Opt Express 20(3):3118–3128. <https://doi.org/10.1364/OE.20.003118>
- Films, F., Berner, N. C., Yim, C., Li, Y., Zhang, X., Chen, Z., ... Wang, J. (2015) Direct observation of degenerate two-photon absorption and its saturation in WS₂ and MoS₂. ACS Nano, 9(7), 7142–7150. <https://doi.org/10.1021/acsnano.5b03480>
- Ganeev RA, Rysanyansky AI, Kodirov MK, Kamalov SR, Li VA, Tugushev RI, Usmanov T (2002) Optical limiting in cobalt-doped polyvinylpyrrolidone. Appl Phys B Lasers Opt 74(1): 47–51. <https://doi.org/10.1007/s003400100753>
- Ganeev RA, Baba M, Morita M, Rau D, Fujii H, Rysanyansky AI, Ishizawa N, Suzuki M, Kuroda H (2004) Nonlinear optical properties of CdS and ZnS nanoparticles doped into zirconium oxide films. J Opt A Pure Appl Opt 6(4):447. Retrieved from <http://stacks.iop.org/1464-4258/6/i=4/a=024>–453
- Ganeev RA, Baba M, Rysanyansky AI, Suzuki M, Kuroda H (2005) Laser ablation of GaAs in liquids: structural, optical, and nonlinear optical characteristics of colloidal solutions. Appl Phys B 80(4):595–601. <https://doi.org/10.1007/s00340-004-1734-9>
- Ganeev RA, Chakravarty U, Naik PA, Srivastava H, Mukherjee C, Tiwari MK, Nandedkar RV, Gupta PD (2007) Pulsed laser deposition of metal films and nanoparticles in vacuum using subnanosecond laser pulses. Appl Opt 46(8):1205–1210. <https://doi.org/10.1364/AO.46.001205>
- Ganeev RA, Suzuki M, Baba M, Ichihara M, Kuroda H (2008) Low- and high-order nonlinear optical properties of BaTiO₃ and SrTiO₃ nanoparticles. J Opt Soc Am B 25(3):325–333. <https://doi.org/10.1364/JOSAB.25.000325>
- Gayvoronsky V, Galas A, Shepelyavyy E, Dittrich T, Timoshenko VY, Nepijko SA, Brodyn MS, Koch F (2005) Giant nonlinear optical response of nanoporous anatase layers. Appl Phys B Lasers Opt 80(1):97–100. <https://doi.org/10.1007/s00340-004-1676-2>
- Golightly JS, Castleman AW, Pennysyl V (2006) Analysis of titanium nanoparticles created by laser irradiation under liquid environments. J PhysChem B 110:19979–19984. <https://doi.org/10.1021/jp062123x>
- Hahn A, Barcikowski S, Chichkov BN, Zentrum L (2008) Influences on nanoparticle production during pulsed laser ablation. J Laser Micro/Nanoeng 3(2):73–77. <https://doi.org/10.2961/jlmn.2008.02.0003>
- Han JB, Chen DJ, Ding S, Zhou HJ, Han YB, Xiong GG, Wang QQ (2006) Plasmon resonant absorption and third-order optical nonlinearity in Ag-Ti cosputtered composite films. J Appl Phys 99(2):1–5. <https://doi.org/10.1063/1.2165410>
- Jeon J-S, Yeh C-S (1998) Studies of silver nanoparticles by laser ablation method. J Chin Chem Soc 45:721–736
- Jiang Y, Ma Y, Fan Z, Wang P, Li X, Wang Y, Zhang Y (2018) Abnormal nonlinear optical properties of hybrid. Opt Lett 43(3):2–5
- Joos JJ, Martin LIDJ, Hens Z, Smet PF (2017) Hybrid remote quantum dot / powder phosphor designs for display backlights. Light: Sci Appl 6(2016):1–9. <https://doi.org/10.1038/lsa.2016.271>
- Jyothi L, Kuladeep R, Rao DN (2015) Solvent effect on the synthesis of cobalt nanoparticles by pulsed laser ablation: their linear and nonlinear optical properties. J Nanophotonics 9(1):93088. <https://doi.org/10.1117/1.JNP.9.093088>
- Kabashin AV, Meunier M (2003) Synthesis of colloidal nanoparticles during femtosecond laser ablation of gold in water. J Appl Phys 94(12):7941–7943. <https://doi.org/10.1063/1.1626793>
- Kaminskiene Z, Prosycevas I, Stonkute J, Guobiene A (2013) Evaluation of optical properties of Ag, Cu, and Co nanoparticles synthesized in organic medium. Acta Phys Pol A 123(1):111–114. <https://doi.org/10.12693/APhysPolA.123.111>
- Karali, T., Can, N., Valberg, L., Stepanov, A. L., Townsend, P. D., Buchal, C., ... Ong, C. (2005) Optical properties and luminescence of metallic nanoclusters in ZnO: Cu. Phys B Condens Matter 363(1):88–95. <https://doi.org/10.1016/j.physb.2005.03.006>
- Lee YH, Yan Y, Polavarapu L, Xu Q, Lee YH, Yan Y et al (2009) Nonlinear optical switching behavior of Au nanocubes and nano-octahedra investigated by femtosecond -scan measurements. Appl Phys Lett 95(23105):023105. <https://doi.org/10.1063/1.3177064>
- Li J, Liu C, Xie Z (2011) Synthesis and surface plasmon resonance properties of carbon-coated cu and co nanoparticles. Mater Res Bull 46(5):743–747. <https://doi.org/10.1016/j.materresbull.2011.01.014>
- Link S, Burda C, Nikoobakht B, El-Sayed MA (2000) Laser-induced shape changes of colloidal gold nanorods using femtosecond and nanosecond laser pulses. J Phys Chem B 104(26):6152–6163. <https://doi.org/10.1021/jp000679t>
- Liu X, Guo S, Wang H, Hou L (2001) Theoretical study on the closed-aperture Z-scan curves in the materials with nonlinear refraction and strong nonlinear absorption. Opt Commun 197(4–6):431–437. [https://doi.org/10.1016/S0030-4018\(01\)01406-7](https://doi.org/10.1016/S0030-4018(01)01406-7)

- Liu W, Xing J, Zhao J, Wen X, Wang K, Lu P (2017) Giant two-photon absorption and its saturation in 2D organic–inorganic perovskite. *Adv Opt Mater* 201601045:1–6. <https://doi.org/10.1002/adom.201601045>
- Liu W, Li X, Song Y, Zhang C, Han X, Long H, Wang B, Wang K, Lu P (2018) Cooperative enhancement of two-photon-absorption-induced photoluminescence from a 2D perovskite-microsphere hybrid dielectric structure. *Adv Funct Mater* 28:1707550. <https://doi.org/10.1002/adfm.201707550>
- Mafune F, Kohno J, Takeda Y, Kondow T (2000) Formation and size control of silver nanoparticles by laser ablation in aqueous solution. *J Phys Chem B* 104:9111–9117. <https://doi.org/10.1021/jp001336y>
- Semaltianos NG (2010) Nanoparticles by laser ablation. *Crit Rev Solid State Mater Sci* 35(2):105–124. <https://doi.org/10.1080/10408431003788233>
- Sheik-bahae M, Said AA, Van Stryland EW (1989) High-sensitivity, single-beam n_2 measurements. *Opt Lett* 14(17):955–957. <https://doi.org/10.1364/OL.14.000955>
- Shukla V, Singh CP, Mukherjee C, Bindra KS (2013) Investigation of optical limiting in cobalt nanoparticles synthesized by laser ablation. *Chem Phys Lett* 555:149–153. <https://doi.org/10.1016/j.cplett.2012.10.035>
- Simakin AV, Voronov VV, Shafeyev GA (2007) Nanoparticle formation during laser ablation of solids in liquids. *Phys Wave Phenom* 15(4):218–240. <https://doi.org/10.3103/S1541308X07040024>
- Simon G, Meziane L, Courty A, Lisiecki I (2016) Low wavenumber Raman scattering of cobalt nanoparticles self-organized in 3D superlattices far from surface plasmon resonance. *J Raman Spectrosc* 47:248–251. <https://doi.org/10.1002/jrs.4782>
- Stepanov AL (2016) Nonlinear optical properties of metal nanoparticles in silicate glass. *Glass Nanocomposites Elsevier Inc.* <https://doi.org/10.1016/B978-0-323-39309-6.00007-9>
- Sugiyama M, Okazaki H, Koda S (2002) Size and shape transformation of TiO₂ nanoparticles by irradiation of 308-nm laser beam. *Jpn J Appl Phys* 41(7 A):4666–4674. <https://doi.org/10.1143/JJAP.41.4666>
- Takami A, Kurita H, Koda S (1999) Laser-induced size reduction of noble metal particles. *J Phys Chem B* 103:1226–1232. <https://doi.org/10.1021/jp983503o>
- Torrell M, Adochite RC, Cunha L, Barradas NP, Alves E, Beaufort MF, Rivière JP, Cavaleiro A, Dosta S, Vaz F (2012) Surface plasmon resonance effect on the optical properties of TiO₂ doped by Noble metals nanoparticles. *J Nano Res* 18–19: 177–185. <https://doi.org/10.4028/www.scientific.net/JNanoR.18-19.177>
- Tsuji T, Iryo K, Watanabe N, Tsuji M (2002) Preparation of silver nanoparticles by laser ablation in solution: influence of laser wavelength on particle size. *Appl Surf Sci* 202:80–85
- Tsuji T, Hamagami T, Kawamura T, Yamaki J, Tsuji M (2005) Laser ablation of cobalt and cobalt oxides in liquids: influence of solvent on composition of prepared nanoparticles. *Appl Surf Sci* 243(1–4):214–219. <https://doi.org/10.1016/j.apsusc.2004.09.065>
- Vall R, Wautelet M, Dauchot JP, Hecq M (2001) Size and segregation effects on the phase diagrams of nanoparticles of binary. *Nanotechnology* 12:68–74
- Wang L, Li Q, Wang H, Huang J, Zhang R, Chen Q et al (2015) Ultrafast optical spectroscopy of surface-modified silicon quantum dots : unraveling the underlying mechanism of the ultrabright and color-tunable photoluminescence. *Light: Sci Appl* 4(2014):1–8. <https://doi.org/10.1038/lsa.2015.18>
- Wautelet M (1998) On the shape dependence of the melting temperature of small particles. *Phys Lett A* 9601:341–342
- Wautelet M, Dauchot JP, Hecq M (2000) Phase diagrams of small particles of binary systems: a theoretical approach. *Nanotechnology* 11:6–9
- Wautelet M, Dauchot JP, Hecq M (2003) Size effects on the phase diagrams of nanoparticles of various shapes. *Mater Sci Eng C* 23:187–190
- Yashunin DA, Korytin AI (2017) Localized Plasmon resonance in metal nanoparticles using Mie theory. *J Phys Conf Ser* 850: 12017. <https://doi.org/10.1088/1742-6596/850/1/012017>
- Yuwono AH, Xue J, Wang J, Elim HI, Ji W, Li Y, White TJ (2003) Transparent nanohybrids of nanocrystalline TiO₂ in PMMA with unique nonlinear optical behavior. *J Mater Chem* 13(6): 1475. <https://doi.org/10.1039/b211976e>
- Zhang J, Lan CQ (2008) Nickel and cobalt nanoparticles produced by laser ablation of solids in organic solution. *Mater Lett* 62(10–11):1521–1524. <https://doi.org/10.1016/j.matlet.2007.09.038>
- Zhang J, Chen TP, Li XD, Liu YC, Liu Y, Yang HY (2016) Investigation of localized surface plasmon resonance of TiN nanoparticles in TiN_xO_y thin films. *Opt Mater Express* 6(7): 2422–2433. <https://doi.org/10.1364/OME.6.002422>
- Zhao JP, Chen ZY, Cai XJ, Rabalais JW, Zhao JP, Chen ZY, Cai XJ (2015) Annealing effect on the surface plasmon resonance absorption of a Ti–SiO₂ nanoparticle composite. *J Vac Sci Technol B* 24:1104–1108